RSC Advances

ROYAL SOCIETY OF CHEMISTRY

www.rsc.org/advances

Immobilization of Metalloporphyrin on the Silica Shell with Bimetallic Oxide Core for Ethylbenzene Oxidation

Sufang Zhao, Yuan Chen, Zhigang Liu*

State Key Laboratory of Chemo/Biosensing and Chemometrics, College of Chemistry and Chemical Engineering, Hunan University, Changsha, Hunan 410082, China

Abstract

In this study, metalloporphyrin has been immobilized on a core-shell structured SiO_2@CeO_2 doped with transition metals such as Fe, Cu, Co and Mn. The as-prepared catalysts have been characterized via N_2 adsorption-desorption, XRD, TEM, FT-IR, and Uv-vis. It is found that metalloporphyrin is anchored onto SiO_2 shell with about 20 nm in size and MO_x/CeO_2 core (M = Fe, Cu, Co and Mn) with about 120 nm in diameter, which may benefit the diffusion of substrates through the pores in the thin shell into the metal oxide cores and the formation of the synergistic effect between metalloporphyrin and metal oxides. Moreover, CoTPP-(MO_x/CeO_2)@SiO_2 catalysts (M=Fe, Cu, Co and Mn) present different physical and chemical properties such as surface areas, particle sizes and catalytic performance, owing to the addition of transition metals into CeO_2. And the catalyst doped with Co exhibits higher catalytic performance than the other catalysts for ethylbenzene oxidation. Thus, the addition of transition metals such as Co, Cu, Fe and Mn plays an important role in the catalytic performance of the catalysts for ethylbenzene oxidation via adjusting the physical and chemical properties of the core-shell catalysts.

Keyword: Immobilization; Metalloporphyrin; Core-shell structure; Bimetal oxide; Ethylbenzene Oixdation

Introduction

There has been a substantial growing interest in applying metalloporphyrin as the model of cytochrome P450 monooxygenases to selective oxidation reactions of chemical compounds under mild conditions[1-3]. However, owing to easy degradation and difficult reuse of unsupported metalloporphyrin, heterogenization through immobilization of metalloporphyrin onto supports is employed to not only solve deactivation of the catalysts, but also provide special micro environment for oxidation reaction by supports[4-6]. These supports may include organic materials (e.g. ion exchange resin[7,8], natural organic macromolecule polymer[9], peptides[10], metal−organic frameworks (MOFs)[11]) and inorganic materials (e.g. silica gel[12,13], zeolite[14,15], montmorillonite[16], alumina[17]).

Thanks to the outstanding properties of core-shell structured materials, SiO_2@CeO_2 is used to support metalloporphyrin. Guo et al.[4] find these catalysts may exhibit comparable higher catalytic performance for hydrocarbon oxidation than their counterpart homogeneous metalloporphyrin. Here, because of the ability in storing and releasing oxygen, CeO_2 is applied to use as the core of the core-shell structured supports[18-24]. Moreover, transition metals are usually added into CeO_2 to enhance catalytic properties of the catalysts by improving the thermal stability and redox properties of CeO_2[25-27]. Blanco et al.[28] prepared low content of Mn-doped CeO_2 composite by co-precipitation method, and found that cerium oxide can make

manganese species stable in high oxidation state with high catalytic activity. Pérez-Alonso et al.[29] obtained a series of Fe-Ce catalyst by co-precipitation method, and found that the samples may form a solid solution of cerium and iron, that is to say, Fe cations dissolved in CeO_2 cubic lattice. The interaction between the cerium-iron displays a higher rate of CO conversion in the synthesis of hydrocarbons in Fischer-Tropsch reactions.

In this study, we synthesized $MO_x/CeO_2@SiO_2$ with a core-shell structure to immobilize metalloporphyrin. The catalytic performance of the as-prepared catalysts for ethylbenzene oxidation with molecular oxygen as oxidant is used to explore the role of MO_x/CeO_2 and the synergistic effect between metalloporphyrin and the MO_x/CeO_2 core. Techniques such as N_2 adsorption-desorption, XRD, FT-IR, UV-vis, TEM and TPR were employed. And the synthesis and reaction schematic diagram is shown in Scheme 1.

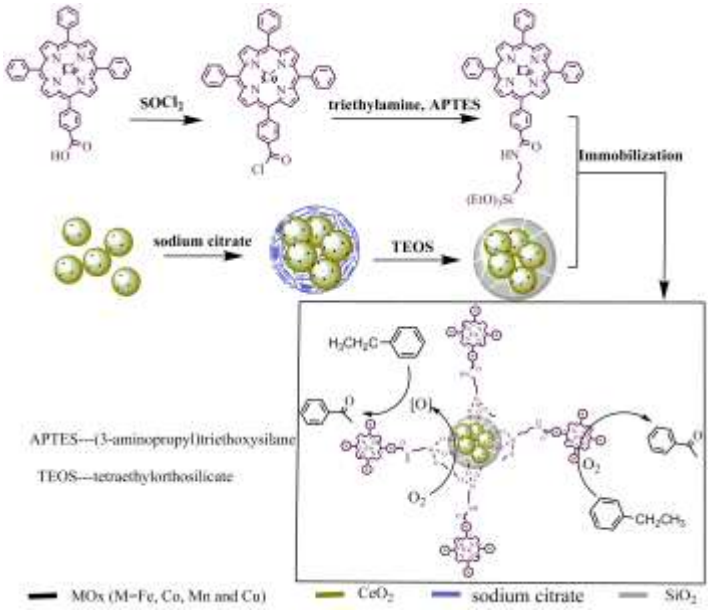

Scheme 1 The synthesis and reaction schematic diagram.

1. Experimental

2.1 Synthesis of cobalt (II) 5-(4-carboxyphenyl)-10,15,20-triphenyl porphyrin (CoTPP)

The compound was synthesized according to the literature[5,30-31]. 220ml of propanoic acid, 5.56 g of benzaldehyde and 2.62 g of 4-carboxy benzaldehyde were added into a three-neck flask and refluxed under stirring, and then 30 mL propanoic acid with 4.69 g pyrrole was dropped through a funnel. The mixture was kept refluxing for 1 h under stirring. The product was cooled overnight, filtered, washed with water, and then purified. 5-(4-Carboxyphenyl)-10, 15, 20-triphenyl porphyrin was obtained. 1.0 g of the obtained porphyrin was dissolved in 100 mL of N,N-dimethylformamide (DMF), and after the addition 2.50 g of $CoCl_2 \cdot 6H_2O$, the mixture was heated to reflux under stirring until the porphyrin was exhausted. After cooling overnight, the solution was filtered and washed repeatedly with deionized water, and the product, denoted as CoTPP, was achieved.

2.2 Synthesis of bimetallic oxides core with silica shell and silica solid

Surface modified FeO_x/CeO_2 was synthesized, according to literatures [32,33]. 0.054 g $FeCl_2 \cdot 3H_2O$ and 1.0786 g $Ce(NO_3)_3 \cdot 6H_2O$ was added into a flask and dissolved in 50 mL of deionized water. Under stirring, NaOH (0.5 g / 50 mL) solution was slowly dropped into the above solution. After stirring for 30 min, the original solution was aged for 18 hours at 80 ^oC. Then the precipitate was filtered and washed with deionized water and anhydrous ethanol for 2 times and then dispersed in 40 mL aqueous solution containing 0.74 g of sodium citrate. After stirring at 90 ^oC for 3 h, the product was centrifugated and then redispersed in 40 mL H_2O, 120 mL anhydrous ethanol and 5 mL ammonium hydroxide before adding 40 mL ethanol solution

containing 0.17 mL tetraethyl orthosilicate (TEOS). The product was centrifugated, washed with ethanol and water and dried after agitating for 6 h at 38 ^{o}C. The coated (FeO_x/CeO_2)@SiO_2 core-shell particles were obtained. Adopting the similar method, other (MO_x/CeO_2)@SiO_2 (M=Mn, Cu, Co) core-shell particles and SiO_2 solid were synthesized.

2.3 Synthesis of CoTPP-(MO_x/CeO_2)@SiO_2 (M=Fe, Cu, Mn and Co) and CoTPP-SiO_2 catalysts

The CoTPP modified with (3-aminopropyl)triethoxysilane (APTES) was prepared according to the literature [4-5, 30], 9 ml of thionyl chloride, 100 mg CoTPP and 30 mL of chloroform ($CHCl_3$) were added into a round bottom flask and refluxed for 3 h under stirring. After the reaction, excess thionyl chloride and chloroform were removed under reduced pressure. The obtained solid mixture was redissolved in 30 mL of chloroform, a mixture of APTES (0.03 g), triethylamine (0.54 g) and chloroform (30 mL) was slowly added into the flask. The reaction was kept refluxing for 1 h.

About 0.24 g of (MO_x/CeO_2)@SiO_2 (M=Co, Cu, Fe or Mn) or SiO_2 was dispersed in 60 mL of toluene under ultrasonication for 20 min at room temperature. The CoTPP modified with APTES was then added dropwise into the flask under vigorous stirring at 75 ^{o}C. The reaction was completed within 24 h and then the precipitate was filtered, washed with toluene and dried under vacuum at 80 ^{o}C. The achieved samples were denoted as CoTPP-(MO_x/CeO_2)@SiO_2 (M=Fe, Cu, Co and Mn).

2.4 Characterization of catalysts

Surface area was measured by nitrogen adsorption/desorption at -196 ^{o}C on an Autosorb-6b apparatus from Quanta Chrome Instruments. The samples were degassed at 100 ^{o}C for 12 h prior to the adsorption experiments. FT-IR spectra were carried out on a Vertex 70 (Bruker) Fourier Transform Infrared spectrometer. UV-vis diffuse reflectance spectra of solid samples were collected on the Shimadzu 2450 spectrophotometer. The morphology of samples was measured by a transmission electron microscopy (TEM, F20) with an electron microscope operating at an 80 kV voltage. The phase analysis of samples was carried out on X-ray Powder Diffraction (XRD-6100).

2.5 Measurement of catalytic performance

Typically, 10 mL ethylbenzene and 30 mg catalyst were loaded in a 50 mL Teflon-lined stainless steel reactor and then sealed and heated to 120 ^{o}C for 5 h under 0.8 MPa O_2 pressure. The sample after reaction are analyzed by gas chromatography (ShimadzuGC-2014 equipped with a capillary column (RTX-5, 30 m, ϕ0.25 mm) with internal standard method using bromobenzene and 1,4-dichlorobenzene as reference. The reused catalyst is obtained through recovering by centrifugation, washing with ethanol and drying at 80 ^{o}C in air.

2. Results and discussion

3.1 BET

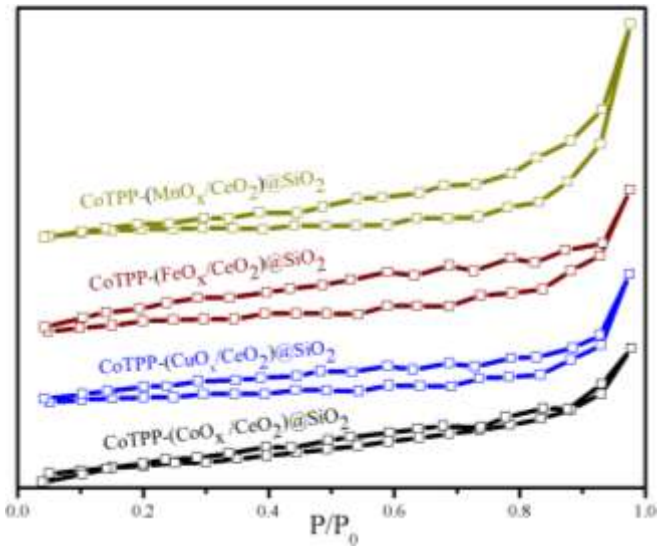

Figure 1 N_2 adsorption/desorption isotherms of CoTPP-(MO_x/CeO_2)@SiO_2 (M=Co, Cu, Fe and Mn) catalysts.

Table 1.The surface area and pore volume of the samples.

Samples	Surface Area/$m^2 \cdot g^{-1}$	Pore Volume/cm^3/g
CoTPP-(FeO_x/CeO_2)@SiO_2	24	0.040
CoTPP-(MnO_x/CeO_2)@SiO_2	16	0.064
CoTPP-(CoO_x/CeO_2)@SiO_2	14	0.035
CoTPP-(CuO/CeO_2)@SiO_2	9	0.034

Figure 1 displays the N_2 adsorption/desorption isotherms of CoTPP-(MO_x/CeO_2)@SiO_2 (M=Co, Cu, Fe and Mn). All the catalysts, as shown in Figure 1, exhibit Typical III shape isotherms[34]. The isothermal lines of the catalysts have the hysteresis loop with the P/P_0 position of the inflection point corresponding to a diameter in the micropores and mesopores, which mean easy diffusion of substrates onto the surface of the metal oxides in the core through the SiO_2 shell and improve the catalytic performance of the samples [34]. Moreover, according to the N_2 adsorption/desorption isotherms, the surface areas and pore volumes of the catalysts are calculated and presented in Table 1. As illustrated in Table 1,

CoTPP-(FeO_x/CeO_2)@SiO_2, compared with CoTPP-(MnO_x/CeO_2)@SiO_2, has a larger surface area (24 $m^2 \cdot g^{-1}$ vs 16 $m^2 \cdot g^{-1}$). However, CoTPP-(MnO_x/CeO_2)@SiO_2 has a pore volume of 0.0636 $cm^3 \cdot g^{-1}$, larger than that of CoTPP-(FeO_x/CeO_2)@SiO_2. This means more mesopores may exist in CoTPP-(MnO_x/CeO_2)@SiO_2 than CoTPP-(FeO_x/CeO_2)@SiO_2. As a result, CoTPP-(CuO_x/CeO_2)@SiO_2 and CoTPP-(CoO_x/CeO_2)@SiO_2, compared with CoTPP-(FeO_x/CeO_2)@SiO_2, have a similar pore volume but lower surface area. It is easy to deduce that CoTPP-(CuO_x/CeO_2)@SiO_2 and CoTPP-(CoO_x/CeO_2)@SiO_2 possesses more mesopores than CoTPP-(FeO_x/CeO_2)@SiO_2. Normally, the existence of mesopores on the shell enables the redox and oxygen storage capability of ceria core doped with transition metal to express and enhance the catalytic performance of the particles for ethylbenzene oxidation.

3.2 XRD

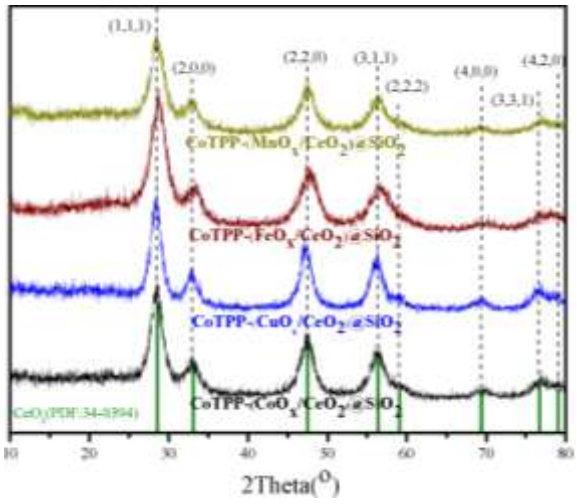

Figure 2 The XRD patterns of CoTPP-(MO_x/CeO_2)@SiO_2 (M= Fe, Cu, Co and Mn) catalysts.

In Figure 2, the characteristic peaks of ceria in the XRD patterns of CoTPP-(MO_x/CeO_2)@SiO_2 (M=Fe, Cu, Co and Mn) are observed at 8.5^o, 33.1^o, 47.5^o, 56.3^o, 59.1^o, 69.4^o, 76.7^o and 79.01^o, which is matched well with the standard

spectrum diagram of cerianite (space groups: Fm-3m, JCPDS no. 34-0394) [29]. Besides these, no more peaks can be found, including the peak of MO_x (M=Fe, Cu, Co and Mn), which may normally be easily observed. This indicates that MO_x (M=Fe, Cu, Co and Mn) are likely present in an amorphous state and/or a relatively high dispersion [38].

The particle sizes of the metal oxides are obtained via the following formula:

$$D_{(h\ k\ l)}=K\lambda/\beta\cos\theta$$

where (h k l) is the plane of ceria, herein we adopt (111) plane, β is the integral half high width which should be converted into radian and θ is the diffraction angle theta. The Scherrer constant K is assumed to be 0.89, and the X-Ray Wavelength λ is set to 0.154056 nm. The theoretical calculation results show that the core of $(CoO_x/CeO_2)@SiO_2$ is assembled by lots of 10.7 nm nanoparticles, and for $(CuO/CeO_2)@SiO_2$, $(FeO_x/CeO_2)@SiO_2$ and $(MnO_x/CeO_2)@SiO_2$, the particle sizes are 9.4 nm, 11.6 nm and 8.9 nm, respectively. It is well established in bimetallic systems that the less reducible metal inhibits the aggregation of the easily reduced metal [28-29,39]. Apparently, these transition metals doped in ceria play a crucial role in the particle sizes of the catalysts .

3.3 TEM

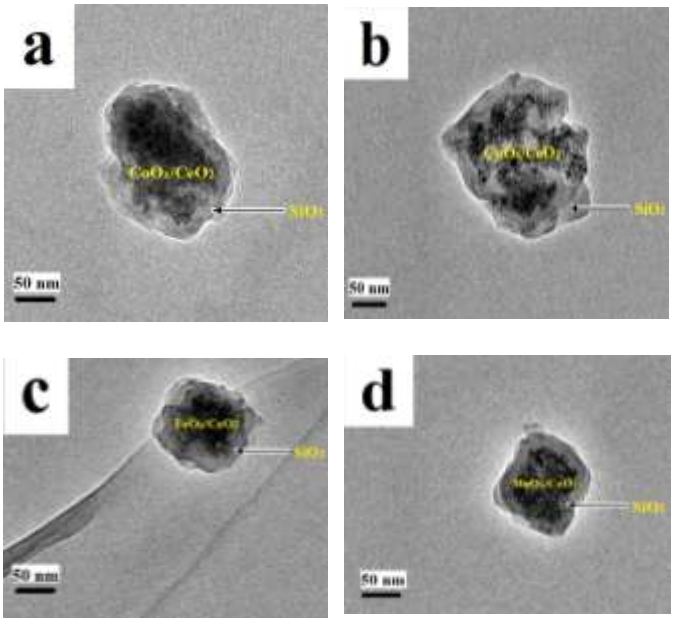

Figure 3 TEM images of (**a**) CoTPP-(CoO_x/CeO_2)@SiO_2, (**b**) CoTPP-(CuO_x/CeO_2)@SiO_2, (**c**) CoTPP-(FeO_x/CeO_2)@SiO_2, (**d**) CoTPP-(MnO_x/CeO_2)@SiO_2.

The TEM images are presented in Figure 3 and the core-shell structure is clearly exhibited. Obviously, it can be found that the bimetallic oxides core is well coated by thin SiO_2 shell with about 20 nm in thickness. However, because of the electrostatic repulsion between the surface of the bimetallic oxide and silica, transition metals doped in CeO_2 particles may have an effect on the formation of core-shell structure, which may cause CeO_2 particles not to be coated by silica shell [4,35,36]. As shown in Scheme 2, we make use of the sodium citrate as surfactant to modify and adjust electrostatic properties of the bimetallic oxides cores, which may benefit the growth of silica to form the core-shell structure [4]. Furthermore, it can be found that the nano metal oxide particles with about 10 nm in diameter as calculated according to the XRD data may accumulate to form larger particles with 120 nm in diameter as measured according to the TEM data. Obviously, a muti-particle core of 120 nm in diameter may come into formation via accumulation of single particles of 10 nm in

size. In this study, the structure of the catalysts with about a 20 nm shell and a 120 nm core in size can enhance the catalytic performance of the core-shell catalysts, for the thin shell may benefit the diffusion of substrates into the metal oxide core. This will lead to the synergistic effect between the metalloporphyrin grafted in the shell and the metal oxides in the core.

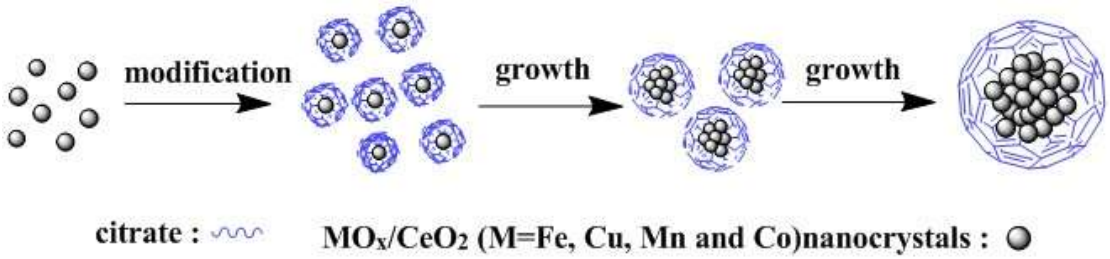

Scheme 2 Formation of citrate-modified MO_x/CeO_2 (M=Fe, Cu, Mn and Co) microspheres.

3.4 FT-IR

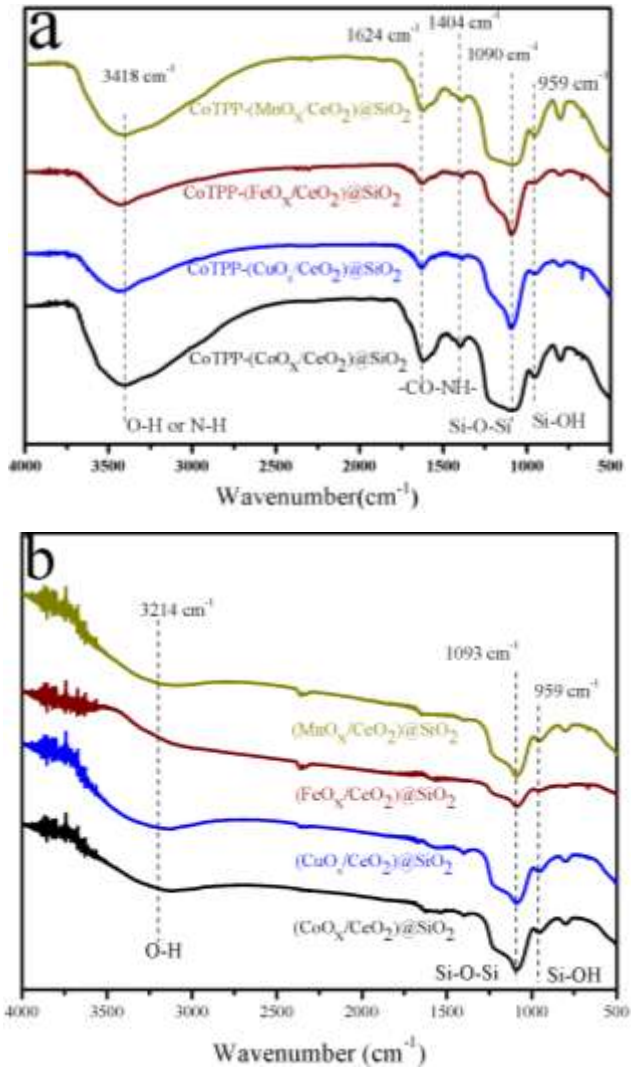

Figure 4 FT-IR spectra patterns of CoTPP-(MO_x/CeO_2)@SiO_2 (**a**) and (MO_x/CeO_2)@SiO_2 (**b**) (M=Co, Cu, Fe and Mn) catalysts.

Figure 4 displays the FT-IR spectra of CoTPP-(MO_x/CeO_2)@SiO_2 (M=Co, Cu, Fe and Mn) catalysts. As shown in Figure 4 (**a**), there is a very large overlapped band at 3418 cm^{-1}, which is ascribed to the bands of adsorption water or N-H group in the sample. In a comparision of Figure 4 (**a**) and (**b**), the adsorption bands observed at 1090 cm^{-1} or lower wavenumbers are ascribed to stretching vibrations of Si-O-Si and Si-O-H in the supports [4,5]. The bands at 1404 cm^{-1} and 3410 cm^{-1} are attributed to bending vibration and stretching vibration of N-H group, respectively[4,5]. In addition, the bands of N-H groups have a blue shift of about 29 cm^{-1}, which may be caused by

the surrounding environment. The adsorption bands, appearing at 1624 cm^{-1} due to the C=O group in amide (N-C=O), demonstrate the formation of amide bonds between metalloporphyrin and the support via dehydrolysis reaction among functional groups of COOH and NH_2 [4,5]. This means metalloporphyrin has been covalently bound to the silica shell. Moreover, FT-IR can only measure the surface properties of the shell not the core in the catalysts and the chemical properties on the shell of the catalysts are evidently similar. Hereafter, there is no difference among the FT-IR spectra of the CoTPP-(MO_x/CeO_2)@SiO_2 (M=Co, Cu, Fe and Mn) catalysts.

3.5 UV-vis

Uv-vis can be used to verify the existence of the porphyrin rings due to their characteristic S and Q bands. For example, cobalt porphyrin, as shown in Figure 5, gives the bands at 414 nm and 532 nm, which are attributed to Soret band and Q band of metalloporphyrin [4-5,30]. As for CoTPP-(MO_x/CeO_2)@SiO_2 (M=Fe, Cu, Co and Mn), there exist two bands at 466 nm and 675 nm when compared with (MO_x/CeO_2)@SiO_2 carriers in Figure 5 (b), which can be ascribed to S and Q bands of immobilized cobalt porphyrin. However, due to the influence of supports, the S and Q bands of immobilized cobalt porphyrin shift to red [37]. It is evident that metalloporphyrin has been anchored onto the supports. What's more, the S and Q bands of CoTPP-(MO_x/CeO_2)@SiO_2 (M=Fe, Cu, Co and Mn) are very similar. This indicates that the cores in the catalysts have little influence on the chemical properties of the metalloporphyrin on the shell, owing to the coating of silica shells.

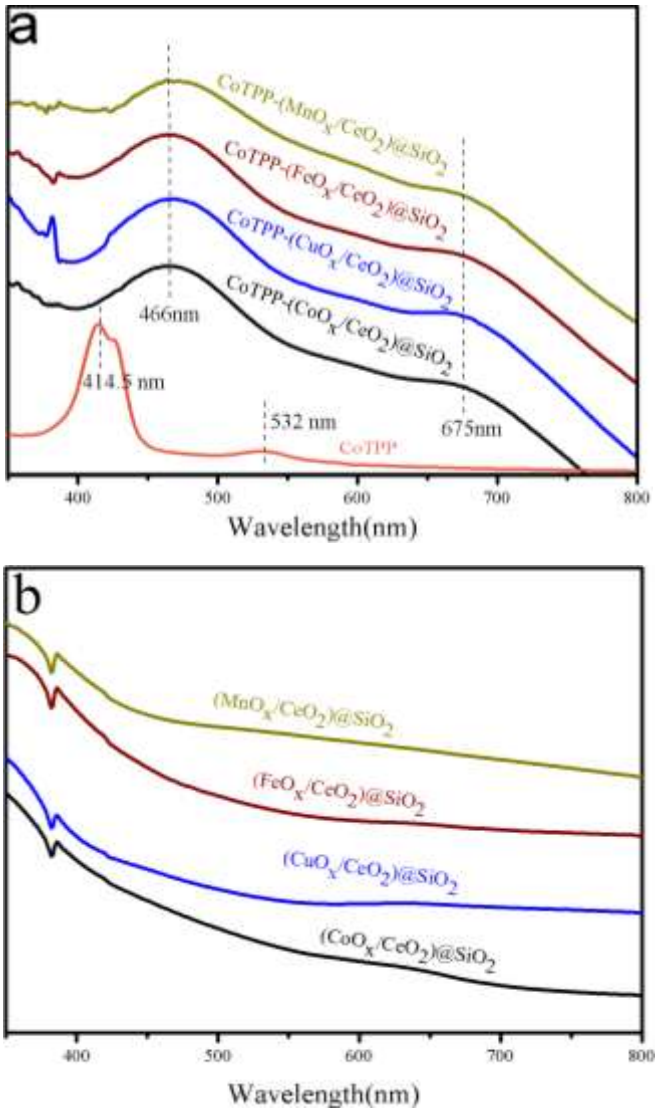

Figure 5 Uv-vis spectra patterns of CoTPP-(MO_x/CeO_2)@SiO_2 (**a**) and (MO_x/CeO_2)@SiO_2 (**b**) samples (M=Co, Cu, Fe and Mn).

3.6 Measurement of the catalytic performance

Selective oxidation of ethylbenzene using molecular oxygen as oxidant is employed to measure the performance of the catalysts. As shown in Table 2, the blank, i.e. autocatalysis system, has the lowest ethylbenzene conversion of 6.9% compared with CoTPP and (MO_x/CeO_2)@SiO_2 (M=Co, Cu, Fe and Mn) catalysts, whose ehtylbenzene conversions reach 9.8%, 13.1%, 13.6%, 17.2% and 13.3%, respectively. Evidently, both CoTPP and (MO_x/CeO_2)@SiO_2 can accelerate the ethylbenzene

oxidation reaction rate to some extent, that is to say that they can enhance the conversion of ethylbenzene.. However, when CoTPP is immobilized on $(MO_x/CeO_2)@SiO_2$ particle to form a CoTPP-$(MO_x/CeO_2)@SiO_2$ catalyst, the activity of the catalyst has been remarkable enhanced. Namely, the ethylbenzene conversion reaches at least up to 28% or even higher in first run. And when compared CoTPP-$(MO_x/CeO_2)@SiO_2$ with CoTPP-SiO_2, the participation of bimetallic oxide (MO_x/CeO_2) increase the conversion of ethylbenzene, obviously. This should be ascribed to the synergistic effect between metalloporphyrin on the shell and the metal oxides in the core. Meanwhile, metalloporphyrin may suffer from leaching and oligomerization during the oxidation reaction, which may results in the deactivation of the catalysts. Herein, it can be clearly observed that the CoTPP-$(MO_x/CeO_2)@SiO_2$ (M=Co, Cu, Fe and Mn) catalysts used up to five times still can remain the selectivity to acetophenone to about 77%, And for CoTPP-$(CoO_x/CeO_2)@SiO_2$ sample, the extent it reduced in ethylbenzene conversion is slower then other samples, so it possesses relatively higher stability and activity for ethylbenzene oxidation. This may be up to the influence of cobalt doping on the physical and chemical properties of the catalyst, such as particle size [39] and redox and oxygen storage capability (OSC) of ceria [40]. As for CoTPP-$(FeO_x/CeO_2)@SiO_2$, the ethylbenzne conversion is almost similar to that of $(FeO_x/CeO_2)@SiO_2$, which suggests the deactivation of CoTPP on the surface of the catalyst. Nevertheless, the ethylbenzene conversions over CoTPP-$(MO_x/CeO_2)@SiO_2$ (M=Co, Cu and Mn) catalysts are higher than those over their corresponding supports. It can be deduced that CoTPP over $(MO_x/CeO_2)@SiO_2$

(M=Co, Cu and Mn) has not been completely deactivated. All in all, the addition of transition metal such as Co, Cu and Mn has a crucial effect on the activities of the catalysts for ehtylbenzene oxidation, owing to their influence on the physical and chemical properties of the catalyst.

Table 2 Comparison of catalytic performance of the catalysts for ethylbenzene oxidation.

samples	R1		R2		R3		R4		R5	
	C (%) [b]	S (%) [c]	C (%)	S (%)	C (%)	S (%)	C (%)	S (%)	C (%)	S (%)
[a] CoTPP-(FeO_x/CeO_2)@SiO_2	28.2	76.6	19.9	77.2	17.3	77.5	16.6	77.1	16.8	78.0
[a] CoTPP-(CuO_x/CeO_2)@SiO_2	30.6	71.4	22.0	77.5	15.2	79.6	14.7	79.7	14.2	78.6
[a] CoTPP-(CoO_x/CeO_2)@SiO_2	28.7	76.8	22.9	77.5	17.6	77.1	17.9	75.2	16.1	77.9
[a] CoTPP-(MnO_x/CeO)@SiO_2	28.8	75.8	17.3	76.0	16.6	76.6	15.3	76.6	15.0	76.3
CoTPP-SiO_2	30.1	75.0	13.2	79.4	11.7	77.6	9.7	77.5	10.2	77.5
[d] (FeO_x/CeO_2)@SiO_2	17.2	74.8	---		---		---		---	
[d] (CuO_x/CeO_2)@SiO_2	13.6	76.4	---		---		---		---	
[d] (CoO_x/CeO_2)@SiO_2	13.1	75.8	---		---		---		---	
[d] (MnO_x/CeO_2)@SiO_2	13.3	75.3	---		---		---		---	
[e] CoTPP	9.8	76.7	---		---		---		---	
Blank	6.9	76.8	---		---		---		---	

Reaction conditions: ethylbenzene 10 mL, O_2 0.8 MPa pressure, temperature 120 °C. [a] 30 mg catalyst, [b] Conversion of ethylbenzene (%). [c] Selectivity to acetophenone (%). [d] 26 mg (MO_x/CeO_2)@ SiO_2. [e] 4 mg CoTPP.

3. Conclusions

In summary, we synthesized CoTPP-(MO_x/CeO_2)@SiO_2 (M=Fe, Cu, Co and Mn) with a core-shell structure. In the catalysts, CoTPP is anchored onto SiO_2 shell with about 20 nm in size and MO_x/CeO_2 core with about 120 nm in diameter, which may

benefit the diffusion of substrates through the pore in the thin shell into the metal oxide cores and the synergistic effect between CoTPP and metal oxides. Moreover, thanks to the addition of transition metals into CeO_2, CoTPP-(MO_x/CeO_2)@SiO_2 (M=Fe, Cu, Co and Mn) present different chemical and chemical properties such as surface areas, particle sizes and catalytic performance. In particular, CoTPP-(CoO_x/CeO_2)@SiO_2 exhibits higher catalytic performance than the other catalysts for ethylbenzene oxidation. Herein, the addition of transition metal such as Co, Cu, Fe and Mn has a crucial effect on the properties of the catalysts for ehtylbenzene oxidation, owing to their influence on the physical and chemical properties of the catalyst.

Acknowledgments

The authors gratefully acknowledge the financial support from National Natural Science Foundation of China (No.21103045, 1210040, 1103312) and the Fundamental Research Funds for the Central Universities.

Corresponding author at: School of Chemistry and Chemical Engineering, Hunan University, Changsha 410082, PR China

Tel.: +86-731-8882-3327.

E-mail address: liuzhigang@hnu.edu.cn (Z. Liu)

Notes and references

1 L. J. Que and W. B. Tolman, *Nature*, 2008, **455**, 333.

2 R. A. Sheldon, *Green Chem.*, 2007, **9**, 1273.

3 D. Mansuy, *Catal. Today*, 2008, **138**, 2.

4 X. Guo, Y. Y. Li, D. H. Shen, J. Gan, M. Tian and Z. G. Liu, *Appl. Catal., A*, 2012, **413**, 30.

5 D. H. Shen, L. T. Ji, Z. G. Liu, W. B. Sheng and C. C. Guo, *J. Mol. Catal. A: Chem.*, 2013, **379**, 15.

6 S. Yuvaraj, M. Gabriele, P. Giuseppe, M. Eugenio, P. Roberto, D. A. Arnaldo and D. N. Corrado, *Adv. Mater. Lett.*, 2012, **3**, 442.

7 T. Ishida, S. Okamoto, R. Makiyama and M. Haruta, *Appl. Catal. A*, 2009, **353**, 243.

8 O. Junichi, M. Masaki, I. Akimasa, K. Tatsuya, H. Hirotaka, M. Noriko, T. Yoshimasa and S. Yutaka, *Anal. Sci.*, 1991, **7**, 555.

9 X. Y. Yang, S. H. Lin and M. R. Wiesner, *J. Hazard. Mater.*, 2014, **264**, 161.

10 C. J. Taggart, E. Z. Welch, M. F. Mulqueen, V. B. Dioguardi, A. G. Cauer, B. Kokona and R. Fairman, *Biomacromolecules*, 2014, **15**, 4544.

11 M. Zhao, S. Ou, and C.-D. Wu, *Acc. Chem. Res.*, 2014, **47**, 1199.

12 F. L. Benedito, S. Nakagaki, A. A. Saczk, P. G. P. Zamora and C. M. M. Costa, *Appl. Catal. A*, 2003, **250**, 1.

13 S. Nakagaki, G. K.B. Ferreira, A. L. Marçal and K. J. Ciuffi, *Curr. Org. Synth.*, 2014, **11**, 67.

14 V. R. Rani, M. R. Kishan, S. J. Kulkarni and K. V. Raghavan, *Catal. Commun.*, 2005, **6**, 531.

15 M. J. F. Calvete, M. Silva, M. M. Pereira and H. D. Burrows, *RSC. Adv.*, 2013, **3**, 22774.

16 A. M. Machado, F. Wypych, S. M. Drechsel and S. Nakagaki, *J. Colloid Interface Sci.*, 2002, **254**, 158.

17 M. R. D. Nunzio, B. Cohen, S. Pandey, S. Hayse, G. Piani and A. Douhal. *J. Phy. Chem. C*, 2014, **118**, 11365.

18 X. W. Liu, K. B. Zhou, L. Wang, B. Y. Wang and Y. D. Li, *J. Am. Chem. Soc.*, 2009, **131**, 3140.

19 L. J. Yang, S. Zhou, T. Ding and M. Meng, *Fuel Process. Technol.*, 2014, **124**, 155.

20 P. Gawade, B. Bayram, A. M. C. Alexander and U. S. Ozkan, *Appl. Catal. B*, 2012, **128**, 21.

21 X. Guo, Y. Y. Li, D. H. Shen, Y. Y. Song, X. Wang and Z. G. Liu, *J. Mol. Catal. A*, 2013, **367**, 7.

22 G. R. Rao, S. K. Meher, B. G. Mishra and P. H. K. Charan, *Catal. Today*, 2012, **198**, 140.

23 Z. L. Wu, M. J. Li, J. Howe, Harry M. Meyer and S. H. Overbury, *Langmuir*, 2010, **26**, 16595.

24 Z. L. Wu, M. J. Li and S. H. Overbury. *J. Catal.*, 2012, **285**, 61.

25 H. Li, G. F. Wang, F. Zhang, Y. Cai, Y. D. Wang and I. Djerdj, *RSC. Adv.*, 2012, **2**, 12413.

26 P. Zhao, C. N. Wang, F. He and S. T. Liu, *RSC. Adv.*, 2014, **4**, 45665.

27 B. K. Cho, *J. catal.*, 1991, **131,** 74.

28 G. Blanco, M. A. Cauqui and J. J. Delgado, *Surf. Interface Anal.*, 2004, **36,** 752.

29 F. J. P. Alonso, M. L. Granados and M. Ojeda, *Chem. Mater.*, 2005, **17**, 2329.

30 X. Guo, D. H. Shen, Y. Y. Li, M. Tian, Q. Liu, C. C. Guo and Z. G. Liu, *J. Mol. Catal. A*, 2011, **351**, 174.

31 Z. G. Liu, L. T. Ji, X. L. Dong, Z. Li, L. L. Fu and Q. A. Wang, *RSC Adv.*, 2015, **5**, 6259.

32 Z. G. Liu, R. X. Zhou and X. M. Zheng, *J. Mol. Catal. A*, 2007, **267**,137.

33 T. Aubert, F. Grasset, S. Mornet, E. Duguet, O. Cador, S. Cordier, Y. Molard, V. Demange, M. Mortier and H. Haned, *J. Colloid Interface Sci.*, 2010, **341**, 201.

34 K. S. W. Sing, D. H. Everett, R. A. W. Haul, L. Moscou, R. A. Pierotti, J. Rouquérol and T. Siemieniewska, *Pure Appl. Chem.*, 1985, **57**, 603.

35 T. Tago, S. Tashiro, Y. Hashimoto, K. Wakabayashi and M. Kishida. *J. Nanopart. Res.*, 2003, **5**, 55.

36 F. Grasset, R. Marchand, A. M. Maric, D. Fauchadour and F. Fajardie, *J. Colloid Interface Sci.*, 2006, **299**, 726.

37 G. Huang, T. M. Li, S. Y. Liu and M. G. Fan, *Appl. Catal. A*, 2009, **371**, 161.

38 Z. G. Liu, S. H. Chai, A. Binder, Y. Y. Li, L. T. Ji and S. Dai, *Appl. Catal. A*, 2013, **451**, 282.

39 Z. Lendzion-Bielun, M. M. Bettahar and S. Monteverdi, *Catal. Commun.*, 2010, **11**, 1137.

40 A. B. Kehoe, D. O. Scanlon and G. W. Watson, *Chem. Mater.* 2011, **23**, 4464.